**Very Long Baseline Interferometry and the VLBA**
**ASP Conference Series, Vol. 82, 1995**
**J. A. Zensus, P. J. Diamond, and P. J. Napier (eds.)**

**Printed June 13, 1995**

CHAPTER 11

# Spectral-Line VLBI

MARK J. REID

HARVARD-SMITHSONIAN CENTER FOR ASTROPHYSICS

**Abstract** The special problems encountered when performing spectral-line VLBI observations are discussed in this Chapter. In particular, the usefulness of Fourier transforming measured visibility data with respect to time, delay or frequency for purposes of fringe detection and calibration is clarified.

## Contents



## 11.1 Spectral Line VLBI Sources

A variety of astronomical sources can be observed with Very Long Baseline Interferometric (VLBI) techniques. The primary observational limitation is that, for a given VLBI array and integration time, there is a minimum brightness temperature for detection. Since, for line observations, bandwidths are limited to the line width of the source (usually less than 100 kHz) a typically minimum brightness temperature (for the VLBA) will be greater than $\sim 10^9$ K. This high brightness temperature requires non-thermal emission processes.

High-brightness spectral lines are achieved in cosmic sources through stimulated emission (masers) and by normal (thermal) absorption of a bright background source (e.g., a compact extragalactic source). Although some effort has been made to observe 21-cm hydrogen absorption against active galactic nuclei, most line-VLBI observations to date involve masers, and this chapter will be limited to these observations. However, the techniques of absorption-line observations are similar to those of emission-line observations, and most of the principles discussed below apply to both types of sources.

Briefly, cosmic sources of maser emission are divided into two classes: interstellar and stellar masers. Interstellar maser sources are found in star forming regions. The masing molecules appear to be remnant interstellar material that did not get incorporated into stars. Widespread and strong interstellar masers include hydroxyl (OH), water vapor ($H_2O$), and methyl alcohol ($CH_3OH$). Stellar masers occur in circumstellar envelopes ejected from red giant and super-giant stars. Thus, the masing molecules are from the star. In addition to hydroxyl (OH) and water vapor ($H_2O$), stellar masers exhibit strong silicon monoxide (SiO) masers.

Most interstellar and stellar masers are associated with highly luminous ($L \sim 10^4\ L_\odot$) objects. A maser source is often composed of dozens of "spots", each at a distinct radial velocity. Spot sizes are usually less than $\sim$ 1 AU and the spots are spread over regions up to about $\sim 10^4$ AU. Each spot demarcates a path through an interstellar cloudlet or section of a circumstellar envelope that is roughly $10^1$ to $10^2$ AU long and contains a mass of molecular hydrogen of roughly ten times the mass of Jupiter.

Since maser spots are very bright, they are often easily detected with VLBI arrays. Maps of the locations and radial velocities of masers can be used to understand the dynamics and physical conditions in the masing regions. Also, proper motions (motions on the plane of the sky) have been measured for interstellar OH and $H_2O$ masers. Thus, the three-dimensional velocity field can be measured, and distances can be directly determined by comparison of the angular (proper) motions and the linear (radial) speeds.

## 11.2 Basic Concepts

The output of an interferometer correlator can be represented as complex numbers (fringe visibilities) on a two-dimensional grid. For a conventional lag (XF) correlator the output is the complex visibility as a function of delay, $\tau$, and time, $t$. The complex visibility, $\rho(t, \tau)$, can be represented as

$$\rho(t_k, \tau_\ell) = c(t_k, \tau_\ell) + i\ s(t_k, \tau_\ell) \ , \tag{11.1}$$

where $c(t_k, \tau_\ell)$ and $s(t_k, \tau_\ell)$ are the "cosine channel" or real part and the "sine channel" or imaginary part of the visibility, respectively. The subscripts denote that these variables, in practice, are not continuously determined, but are measured at discrete values. After correlation the delay function (at any point in time) can be Fourier transformed to yield a source spectrum. For an FX correlator, such as the VLBA correlator, a short time-series of voltages from two telescopes are first Fourier transformed and then cross-correlated. The output is then the complex visibility as a function of frequency (or Doppler velocity) and time. For either correlator, the *time sequence* of complex visibilities can be Fourier transformed to yield the fringe frequency or fringe rate. Thus, using Fourier transforms in the delay and/or (post-correlation) time domain, the complex visibility data can be thought of occupying four "data planes".

The complex fringe visibilities for a continuum and spectral line source are schematically illustrated in figures 11.1 and 11.2, respectively, on the four data planes. Along each axis we show typical interferometric responses. The interferometric visibilities are complex numbers. These are difficult to portray graphically, and, with the exception of the time axis, we show only the magnitude (or amplitude) of the visibility along each axis. For the time axis we indicate the variations of the real and imaginary components with solid and dashed lines, respectively. As mentioned above, a conventional XF correlator yields visibilities in the delay–time domain (plane "a") and the VLBA FX correlator yields visibilities in the frequency–time domain (plane "c"). Given the data in any one of the 4 planes, one can manipulate, via Fourier transforms, the data to any of the remaining 3 planes as needed to simplify the analysis. The detection of a signal is usually most easily accomplished when all the power is concentrated in a few pixels of one of the data planes.

Consider, for example, the problem of detecting a continuum source (e.g., in figure 11.1) with an interferometer. Such a source fills the receiving band and, as such, has a narrow delay function. For a rectangular bandpass and a flat spectrum source, the real part of the delay function is proportional to the Fourier transform of the rectangular bandpass given by

$$c(\tau_\ell) \propto \frac{\sin(2\pi B\tau_\ell)}{(2\pi B\tau_\ell)} \ , \tag{11.2}$$

where $B$ is the frequency width of the bandpass and $\tau_\ell$ is the delay value. The imaginary part of the delay function is given by

$$s(\tau_\ell) \propto \frac{\sin^2(\pi B\tau_\ell)}{(\pi B\tau_\ell)} \ , \tag{11.3}$$

For delay "channel" spacings of $\frac{1}{2B,}$ there are two channels between nulls in the real or imaginary portions of the complex fringe visibility. It can be easily shown that the magnitude (amplitude) of the delay function (i.e., $\sqrt{c^2+s^2}$) is $\sin(\pi B\tau_\ell)$ / $(\pi B\tau_\ell)$ with a width between first nulls of about 4 delay channels. See Thompson, Moran and Swenson (1986) for more details.

In the time domain, the fringe visibility oscillates sinusoidally at the residual fringe rate (i.e., the difference between the source fringe rate and the processor or modeled fringe rate). If one Fourier transforms the time series of visibilities in each delay channel, one replaces the time axis of plane "a" with the fringe rate axis of plane "b". The fringe rate function ideally is a delta function and usually

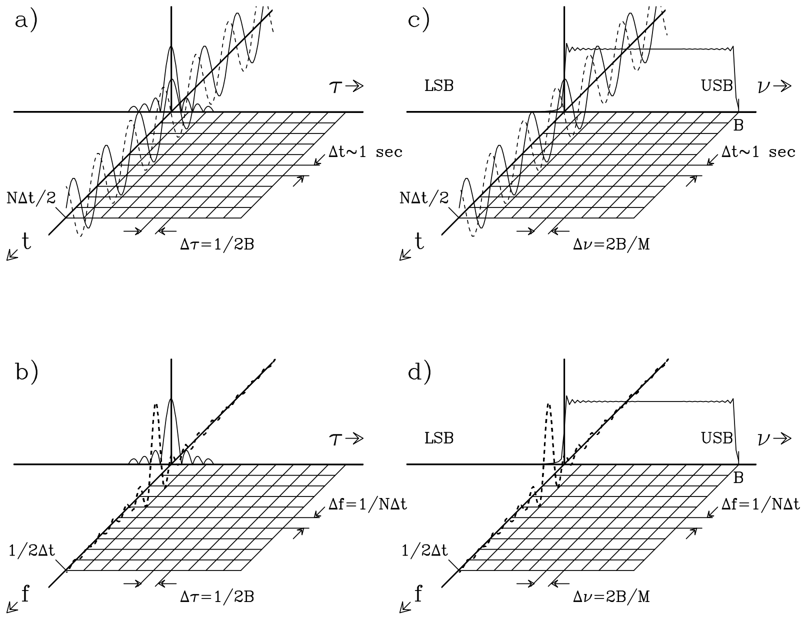


**Figure 11.1:** Fringe visibilities for a continuum source *(see text)*.

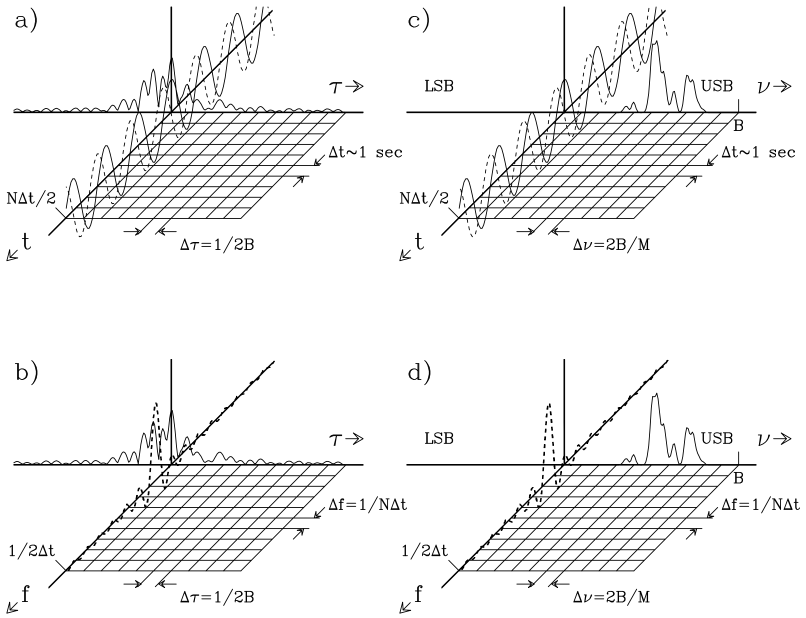


**Figure 11.2:** Fringe visibilities for a spectral-line source *(see text)*.

is quite narrow, provided that the time series of visibilities is shorter than the coherence time of the interferometer. Thus, in plane "b", the fringe visibility amplitude for a continuum source peaks sharply in both axes and is most easily detected there. Fringe fitting of continuum sources, therefore, is usually done in the delay–fringe rate plane.

Alternatively, the narrow-band nature of a spectral-line source suggests a different approach for detection with an interferometer. Such a source has its power naturally concentrated in the frequency domain. Since the Fourier transform of a narrow function is broad, a source with a narrow frequency spectrum has a *broad* delay function. The spectral-line source shown in figure 11.2 is a blend of about 20 narrow components spread over about 1 MHz bandwidth, and hence has narrower delay function than would be found for any one of the components individually. In the time domain, the fringe visibility oscillates sinusoidally, as it does for a continuum source, and if one Fourier transforms the time series of visibilities in each frequency (spectral) channel, one replaces the time axis of plane "c" with the fringe rate axis of plane "d". Thus, in plane "d", the fringe visibility amplitude of a narrow line source peaks sharply in both axes and is most easily detected there. Fringe fitting of spectral-line sources, therefore, is usually done in the frequency–fringe rate plane.

Often one wants to "condition" interferometer data by shifting delay functions (e.g., to correct for clock errors), shifting frequencies or velocities (e.g., to correct for time varying Doppler shifts), or to change spectral resolution or numbers of spectral channels. As for the detection or fringe fitting problem, each conditioning operation is usually most easily accomplished in one of the four visibility planes.

For example, shifting in delay is often necessary to correct for clock errors. Usually the desired shifts are not integral multiples of the delay channel spacings, and, hence, the shifts require interpolation between channels. By use of the shift theorem for Fourier transforms, a shift in one domain results in a linear phase slope in the other domain. Thus, delay shifts are most easily accomplished in the frequency domain as follows:

1. Fourier transform from the delay axis (in either plane "a" or "b") to a frequency axis (in plane "c" or "d").

2. Multiply the frequency functions (spectra) by $e^{i2\pi\nu_n\Delta\tau}$, where $\nu_n$ is the (video) frequency of the n$^{th}$ channel and $\Delta\tau$ is the desired delay shift.

3. If needed, Fourier transform back to the delay domain.

For a line source, the shape of the spectrum in the frequency domain can be arbitrarily complicated. Indeed, the spectrum shown in figure 11.2 was generated by blending many narrow lines with different visibility phases, corresponding to different positions on the sky. However, consider a single, narrow (spectrally unresolved) line. In either a XF or a FX correlator, a finite delay function or a finite time series is Fourier transformed into a spectrum. If no weighting function is applied to the data before transforming (i.e. "uniform weighting"), this is equivalent to multiplying the *complete* delay function (or time series) by a rectangular step function that is zero outside the transform range and one inside that range. Since the Fourier transform of a product of two functions is the convolution of the Fourier transform of each function, this procedure results in convolving the true source spectrum with a "window" function. For uniform weights, the window function is the Fourier transform of the rectangular weighting function and is (as for the delay function for a continuum source mentioned above) a $\sin(x)/x$ function. This leads to both positive and negative spectral "side-lobes" in the frequency and fringe rate axes. Alternative weighting functions, such as Hanning weighting, can reduce side-lobe levels at the expense of degrading the resolution.

## 11.3 Spectral-Line Calibration

I now will outline how a typical spectral-line VLBI observation is conducted and analyzed. This hypothetical observing program will follow a repeated sequence in which a compact continuum source, whose position is accurately known, is observed for a brief period of time, followed by a spectral-line source, which is usually observed for a longer duration. Continuum sources, or calibrators, will be used to determine the behavior of the station clocks, and they can also be used to solve for baselines and atmospheric parameters. In addition, the continuum sources can be used to obtain "off-source" time for total-power (auto-correlation) analysis. Since the continuum sources usually have no detectable emission and absorption lines at the maser frequencies, the autocorrelation spectrum on such a source yields the amplitude response of the bandpass and allows one to generate "on-off/off" total-power spectra for calibration purposes.

For simplicity, and because most VLBI data has been processed with XF correlators, I will assume that the output of the correlator will be a set of cross-correlation and auto-correlation functions for each correlator integration period, $\Delta t$, of typically $\sim$ 1 sec. Thus, the data start as represented by plane "a" of figures 11.2 and 11.1. Data analysis proceeds as described below.

### 11.3.1 Instrumental Parameters

First we find various instrumental parameters responsible for phase shifts in the complex fringe visibilities. If these phase shifts are not removed from the data they will degrade the quality of the line (channel) maps and any astrometric measurements. Commonly the instrumental parameters involve the time variation of the clock at each telescope (often modeled as a linear function of time), the electronic phase differences among video bands, and the phase variations across each video band. In some cases, station coordinates (baselines) and atmospheric models are corrected based upon the calibrator observations.

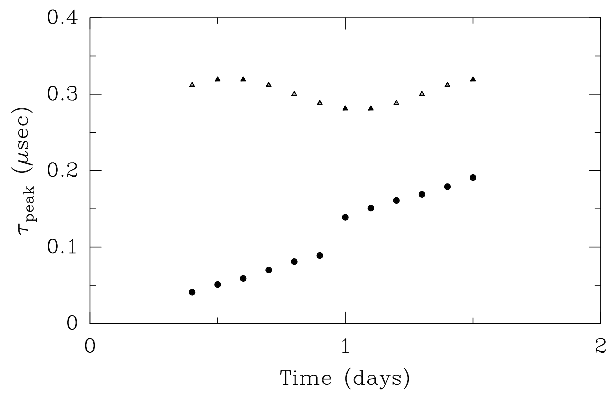


**Figure 11.3:** Interferometer delay versus time. Filled circles show typical behavior reflecting a relative clock drift of $\approx 0.1\mu$sec/day and a clock jump (discontinuity), possibly caused by a station power failure. Filled triangles show a sinusoidal variation with a 24 hour period, indicating a significant parameter error in the correlator model.

Most of the necessary calibration information can be obtained by fitting fringes to the continuum data. This is most easily accomplished by Fourier transforming the time axis of plane "a" to the fringe-rate axis of plane "b", concentrating all the "fringe power" contained in the time spanned by the Fourier transform in a few fringe-rate pixels. Next one finds, via a suitable fitting algorithm, the peak in the delay–fringe rate plane. With perfect clocks, baselines, and atmospheric model parameters, the VLBI processor would exactly compensate for the delay and fringe-rate of the interferometer, and the fringe power would peak in the zero-offset channels of the delay–fringe-rate plane. If the fringes do not peak there, the residual interferometer delays are not zero and post-correlation corrections may be necessary. Shifts in the station clocks will manifest themselves as a shift in the location of the peak in the delay function. Clock drifts, baseline errors, and atmospheric variations result in both delay and fringe-rate offsets. Figure 11.3 provides two examples of the time variation of the residual interferometer delay, both requiring correction. Finally, electronic phase-shifts among bands, caused largely by mismatched low-pass filters and IF mixers, can be determined directly by comparison of the peaked fringe *phase* measured simultaneously among bands on a strong calibrator.

### 11.3.2 Doppler Tracking

We now shift attention to the data from the spectral-line source. Soon we will want to Fourier transform these data from the delay domain of plane "a" to the frequency domain of plane "c". However, there is a correction that is commonly needed and which is most conveniently done in plane "a". During an observation the frequency (or Doppler velocity) of a given spectral line will change, owing to the commonly used procedure of using fixed local oscillators and the presence

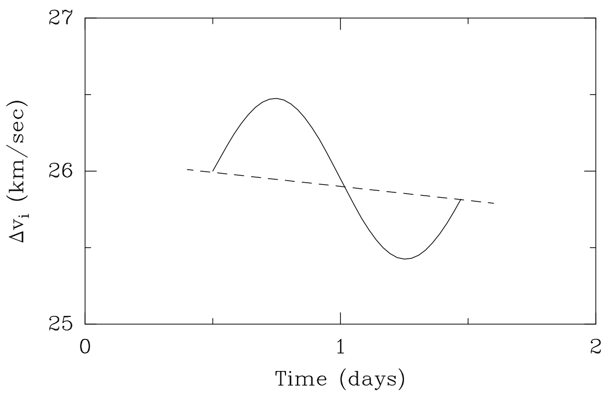


**Figure 11.4:** Doppler velocity of a radio source caused by the rotation of the earth (solid line) and the earth's orbit around the Sun (dashed line). The earth's orbital velocity, projected along the line-of-sight to the radio source, can approach 30 km/sec; while the earth's rotation, similarly projected, can approach 0.5 km/sec.

of frequency changes in the signals caused by rotation of the earth and its orbit about the Sun (e.g., figure 11.4). If the correlator does not correct for these effects (so-called Doppler tracking), it is important to do so in the post-correlation processing. Otherwise a spectral line will slowly drift across the spectrum, degrading the spectral resolution in a systematic, time-dependent, fashion.

One can frequency-shift data by multiplying the delay functions by $e^{i2\pi\Delta\nu\tau_\ell}$, where $\Delta\nu$ is the desired frequency shift and $\tau_\ell$ is the delay value:

$$\rho(t_k, \tau_\ell) \leftarrow \rho(t_k, \tau_\ell)\ e^{+i2\pi\Delta\nu\tau_\ell}\ . \tag{11.4}$$

In this and subsequent relations, the left arrow ($\leftarrow$) is equivalent to an equal sign in FORTRAN and indicates that the value of the right-hand side replaces that of the left-hand side. If $\Delta\nu$ as a function of time is calculated correctly, this correction will hold the spectral line steady in a given spectral channel for the entire observation period, once the data are Fourier transformed from the delay to the frequency domain (plane "c").

### 11.3.3 Transforming from Delays to Frequencies

Once all necessary calibration information has been obtained from the delay data, and Doppler tracking corrections have been made to the line source data, it is time to Fourier transform the data set to the frequency–time domain. The complex fringe visibilities in the delay domain, $\rho(t_k, \tau_\ell)$, are transformed to spectra, $S(t_k, \nu_n)$, by a discrete Fourier transform:

$$S(t_k, \nu_n) = \frac{1}{\mathrm{M}} \sum_{\tau_\ell = -\mathrm{M}\Delta\tau/2}^{+\mathrm{M}\Delta\tau/2} \rho(t_k, \tau_\ell)\ e^{+i2\pi\nu_n\tau_\ell}. \tag{11.5}$$

(Usually a Fast Fourier transform (FFT) algorithm is used to speed up this calculation.) While previous VLBI correlators have usually produced delay functions, the VLBA correlator performs the Fourier transform on-line (before cross-correlating) and also is capable of correcting for the rotation of the earth when Doppler tracking sources. Thus for the VLBA case, the steps described in sections 11.3.2 and 11.3.3 are handled in the correlator.

### 11.3.4 Spectral Line Amplitude Calibration

The interferometer spectra in plane "c" are in "correlation-coefficient" units: that is, they are an effective interferometer antenna temperature divided by a system temperature. We wish to convert these to flux density units (e.g., Janskys) by calibrating the gain of the antennas, the system temperature of the receivers, and the effects of atmospheric emission and attenuation. For most continuum applications this is done by multiplying the correlation data by an effective system temperature (corrected to above the earth's atmosphere), $T^*_{sys}$, and the antenna gain, $Q$ (in units of Jy/K). For an unpolarized source, $Q = 2k/A_{eff}$, where $k$ is Boltzmann's constant and $A_{eff}$ is the effective collecting area of the antenna.

In the absence of digitization and sampling losses in the correlator, the product $T^*_{sys}Q$, the system equivalent flux density (SEFD) in Janskys, scales correlation coefficients to fringe amplitudes in Janskys. For interferometers, as opposed to single antennas, the scaling is done by multiplying the correlation coefficients by the *geometric mean* of the system temperatures in Janskys of the two antennas that were cross correlated. Explicitly,

$$S_{ij}(Jy) = b\,\sqrt{(T^*_{sys}Q)_i\;(T^*_{sys}Q)_j}\;S_{ij}(correlator), \tag{11.6}$$

where $b$ compensates for digitization and sampling losses, and $i$ and $j$ indicate the cross-correlation of the signals from the $i^{th}$ and $j^{th}$ antennas, respectively. For most continuum VLBI applications, the effective system temperatures ($T^*_{sys}$) are measured by comparison of the total-power level on-source when a noise (cal) source of known temperature is switched on and off. Similarly, the gain ($Q$) of each antenna is measured by comparing the total power level on- and off-source (using the program source if it is strong enough), also with the aid of the noise source.

For spectral-line applications, it is often possible to measure directly the SEFD in Janskys ($T^*_{sys}Q$) from the *auto*-correlation spectra *on* and *off* the line source. First, one generates a total-power spectrum, $S(\nu_n)$, in the standard manner used for single-antenna spectral observations (see figure 11.5):

$$S(\nu_n) = \frac{S^{on}(\nu_n) - S^{off}(\nu_n)}{S^{off}(\nu_n)}, \tag{11.7}$$

where $S^{on}(\nu_n)$ and $S^{off}(\nu_n)$ are the raw on– and off–source auto-correlation spectra, respectively. This total-power spectrum will have "correlation coeffi-

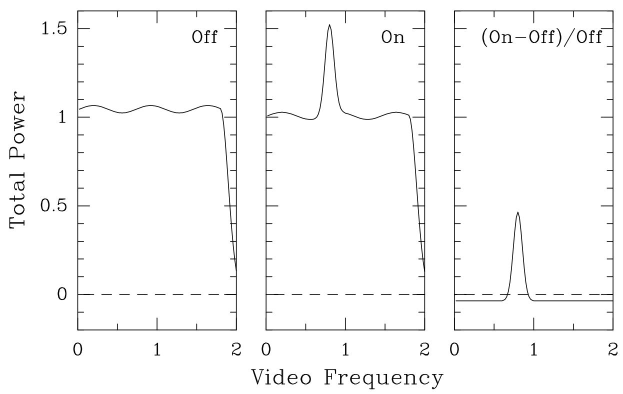


**Figure 11.5:** Total-power spectra from clipped (1-bit sampled) data. Shown is the power versus video frequency for a single telescope pointed off (left panel) and on (middle panel) a maser source. The off-source spectrum displays typical filter response including baseline ripple and high frequency roll-off. The normalized, total-power spectrum, formed by differencing the on- and off-source spectra and dividing by the off-source spectrum (right panel), is corrected for filter response and is proportional to the true source spectrum. Both the off- and on-source spectra have "unity" average value, since they are derived from clipped signals whose zero-delay auto-correlation value is unity, and hence the "on-off/off" spectrum has zero area (and a baseline level below zero).

cient" units and will be sensitive to telescope gain, system temperature, and atmospheric emission and absorption. For example, a spectral line in the total-power spectrum will have a lower strength if the antenna gain decreases, perhaps owing to a pointing error, or if the system temperature increases because a cloud passes over the antenna. One can quantify this performance change by comparing a total-power spectrum from each antenna for each observing scan against a single "template" total-power spectrum of the source. Often the template spectrum is obtained from the largest and best calibrated antenna used in the VLBI array. Each total-power spectrum is stretched (or shrunk) in amplitude until it best matches the template spectrum. The stretching (or shrinking) factor is directly proportional to the desired SEFD ($T^*_{sys}Q$). Indeed, if the template spectrum is properly calibrated in Janskys, the stretching factor is precisely $T^*_{sys}Q$.

Obtaining the gain calibration information for each antenna from its auto-correlation data has been widely used for spectral-line observations. It does require that some off-source observing time be scheduled into the program (and the data recorded on the VLBI tapes). Often one can use the observation time on continuum calibration sources for off-source data, since these data are only used to determine the shape of the passband. Fitting auto-correlation spectra can be an extremely precise method of achieving the *relative* calibration of fringe amplitudes among the antennas of a VLBI array. (*Absolute* calibration depends on the accuracy of the flux density scale assigned to the template spectrum.) Of course, it is important that sufficient signal-to-noise be achieved in the auto-correlation spectra. For a strong maser source precisions of better than 1% are common.

Potential problems with this technique are those that affect most single-dish spectroscopy and include "birdies" (interference) and spectral baseline ripples. Indeed, if auto-correlation data from the continuum calibration sources are used to construct "off-source" spectra, baselines may be poor as the on- and off-source spectra may not be acquired in angular or temporal proximity. Also, there is one subtle electrical problem that is not detected with auto-correlation. If the local oscillator used at the VLBI station does not have a pure "delta function" signal, but has power elsewhere (e.g., in 60 Hz harmonics), then the cross-correlated signal will be reduced (e.g., 60 Hz is outside the "fringe window" of data averaged to $\approx$ 1 second in the correlator). However, the auto-correlation signal will not be reduced, since all the power will usually be contained within one spectral channel (typically many kHz wide).

The auto-correlation data can be useful for more than calibration, since they indicate the total-power emitted by the source (at least all the power within the single antenna beam, which usually is arc-minutes in size). Interferometric data generally do not sample short baseline spacings. For connected-element interferometers like the VLA this occurs because antennas cannot get closer together than the distance at which they touch. For VLBI data the shortest spacings by definition are large (e.g., hundreds of kilometers). One can, in principle, add in the auto-correlation data at the center of the $(u, v)$-plane (i.e."zero spacing" data) in the mapping step. However, in practice this is useful only if the fringe amplitudes on shorter VLBI spacing have a reasonable fraction of the total-power flux density.

### 11.3.5 Clock and Coordinate Corrections

Now the data are in the frequency–time domain (plane "c"); they have been *amplitude* calibrated and are in units of Janskys. It is time to correct the visibility *phases* for various instrumental and propagation effects. Any errors in the station clocks, as well as possible coordinate errors in the locations of the antennas, will lead to time-dependent delay shifts. A delay shift appears as a translation along the $\tau$-axis in data planes "a" and "b". After Fourier transforming the delay ($\tau$) to the frequency axis ($\nu$), *a delay shift appears as a linear frequency-dependent phase change.*

From the calibration information obtained in section 11.3.1, we can generate a table of (or formulae for) the desired delay corrections to be applied to each interferometer baseline at any observing time. The complex fringe visibility spectrum, $S(t_k, \nu_n)$, can be corrected for a delay shift, $\Delta\tau$, as follows:

$$S(t_k, \nu_n) \leftarrow S(t_k, \nu_n)\ e^{-i2\pi\Delta\tau\nu_n}. \tag{11.8}$$

This process removes a phase slope across the video band caused by the delay error.

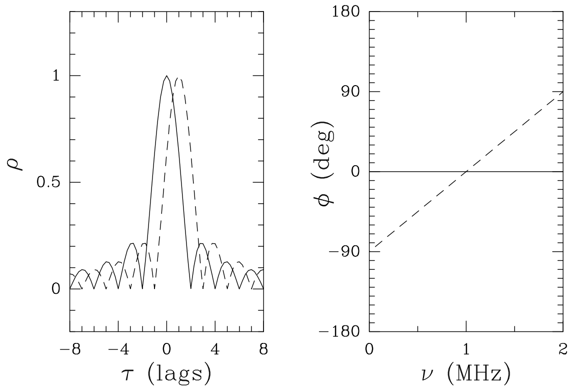


**Figure 11.6:** Interferometer correlation functions (left panel) and associated phase response versus video frequency (right panel). Shown are two cases in which the residual (post correlation) delay has (1) zero offset (solid line) and (2) a 0.25 $\mu$sec offset. A 2 MHz video bandwidth and 1/4 $\mu$sec delay steps are assumed. Note that a residual delay error of one delay step results in a phase slope of 180 degrees across one video sideband.

If delay corrections involve only a correction for a *constant* clock offset at each station, then one can skip to the next step in the calibrations process. However, if, for example, the station clocks drift in time (caused by a frequency error in the oscillator driving the clock), or coordinate corrections are needed, then one must also correct the visibility phase by a video-frequency *independent* amount as follows:

$$S(t_k, \nu_n) \leftarrow S(t_k, \nu_n)\ e^{-i2\pi\Delta\tau\nu_0}, \tag{11.9}$$

where $\nu_0$ is the local oscillator frequency, or sky frequency of the zero video-frequency channel, of the observing band.

One other calibration step is associated with clock or coordinate corrections. When any time-dependent phase correction is made, the original data probably had a non-zero residual fringe-rate. Such data have been degraded in amplitude because they were time averaged (in the correlator) over a portion (hopefully small) of the fringe-rate cycle. Averaging of the fringe visibility, $S(t,\nu)$, which varies in time sinusoidally at a fringe-rate, $f$, decreases its amplitude by a factor given by $\sin(\pi f T)/(\pi f T)$, where T is the integration or averaging time. Thus, when one makes time-dependent phase corrections (equivalently fringe-rate corrections), one should also consider correcting fringe amplitudes by the reciprocal of this "$\sin(x)/x$ " function. Of course, such a correction can only be done correctly for one position on the sky (i.e., the phase center of the map).

### 11.3.6 Electronic Phase Shifts

Many spectral-line and continuum VLBI observations use a number of narrow bands recorded separately on tape to span a wider bandwidth on the sky. Combining the fringe visibilities from different bands requires correcting the data for the visibility phase differences among the bands. Such phase differences are primarily caused by the use of different IF mixers and different electronic components in the low-pass (video) filters following the final mixing stage. The calibration data compiled in section 11.3.1 is now applied to the bands to align their phases to that of a single (reference) video band. This is accomplished as follows:

$$S(t_k, \nu_n) \leftarrow S(t_k, \nu_n)\; e^{-i(\phi^N - \phi^R)}, \tag{11.10}$$

where $(\phi^N - \phi^R)$ is the *band-averaged* phase difference between video band "$N$" and the reference video band "$R$".

Now that the *band-averaged* phases for all video bands are aligned, one can consider correction for the (typically $\sim 10°$) phase ripples across each individual band. This is usually done only for very precise astrometric measurements where very high dynamic range is needed in the channel maps. The phase ripple in each band can be seen on a single scan on a very strong continuum source. Such a correction is accomplished, mathematically, as follows:

$$S(t_k, \nu_n) \leftarrow S(t_k, \nu_n)\; e^{-i\phi^N(\nu)}, \tag{11.11}$$

where $\phi^N(\nu)$ represents the phase as a function of frequency across video band "$N$".

### 11.3.7 Phase Referencing

At this point the data are in the form of amplitude calibrated spectra (in plane "c"), and they have been corrected for clock and coordinate errors and electronic phase shifts. Were this VLA data, taken in a small configuration under good weather conditions, all that would remain to do would be to apply a slowly varying phase correction, determined from continuum calibrator scans, to remove the effects of visibility phase fluctuations caused by the *difference* in the propagation of the radio waves through the earth's atmosphere for the different antennas. However, VLBI data usually contains very large atmospheric phase fluctuations (since the atmospheric fluctuations are largely uncorrelated among the antennas) and an additional term owing to the use of *independent* local oscillators for each antenna. Therefore, most VLBI data must be "phase referenced" in some manner.

For continuum VLBI data the usual procedure is to attempt "self-calibration." This procedure uses the signals from the program source itself, coupled with some knowledge of the source structure, to iteratively solve for the atmospheric or local oscillator phase fluctuations as well as the source structure. However, for spectral-line VLBI and, in particular, for observations of cosmic masers, one can often use the phase variation from a spectral channel containing simple source structure as a reference. Ideally one desires a strong, unblended

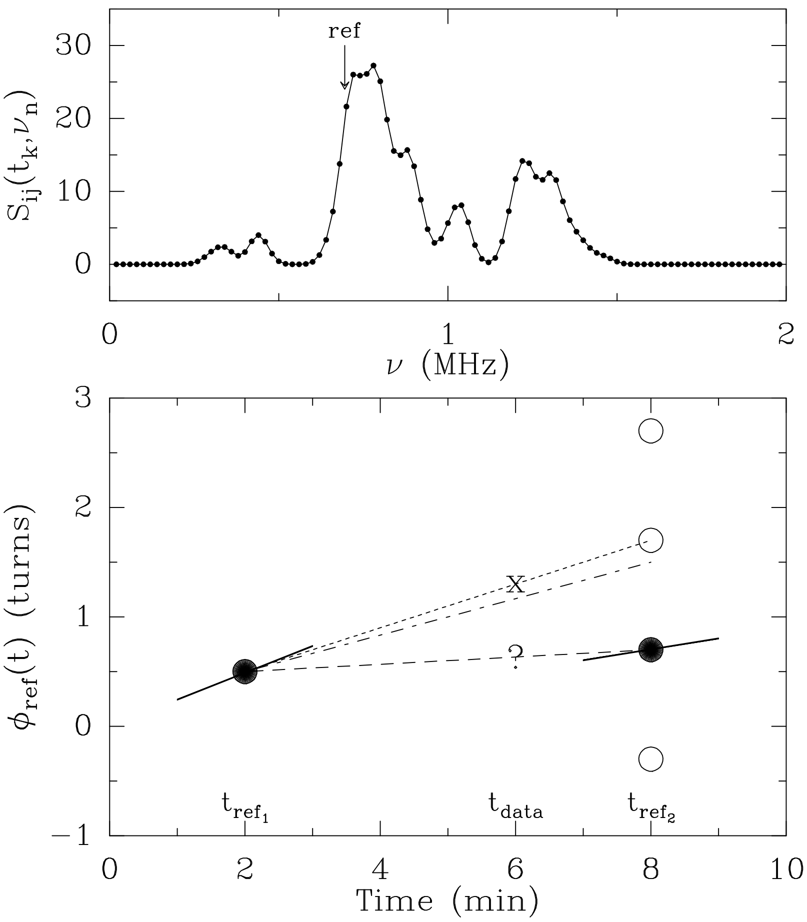


**Figure 11.7:** Phase-referencing. *Top:* Interferometer spectrum indicating a ("ref") channel to be used as a phase reference. *Bottom:* Interferometer phase vs time. Solid circles indicate the phase, arbitrarily defined between 0 and 1 turn, derived by fringe fitting data from the "ref" channel at times $t_{ref_1}$ and $t_{ref_2}$. Heavy lines through the solid circles indicate the fitted fringe rates. The dashed line is a direct connection of the two fitted phases; "?" denotes phase interpolated via this connection at time $t_{data}$. This phase connection and the interpolated phase are incorrect. Phases have integral-turn ambiguities and could be as indicated by the open circles. Averaging the fringe rates from the two fits suggests that the phase should be extrapolated along the dash-dotted line and that, relative to the phase at $t_{ref_1}$, the phase at $t_{ref_2}$ should be one turn higher (i.e., 1.7 turns). This resolves the turn ambiguity between the two times. The best interpolation should follow the dotted line, yielding the phase indicated by the "x" for data at time $t_{data}$.

spectral component as a reference. This may not be available, but the steep edge of a blend of lines (as in figure 11.7) often provides an adequately clean signal. In any event, one can "self-calibrate" the reference channel data, if needed, to correct for complex structure in that spectral channel.

For simplicity, assume that spectral channel "r", at frequency $\nu_r$, contains a strong signal from a single point source on the sky. We copy the visibility spectra, $S(t_k, \nu_r)$, from this channel in plane "c", into a temporary data base, and Fourier transform (the time domain into the fringe-rate domain) to plane "d". We fringe-fit this data over a time period (typically minutes) long enough to provide an adequate signal-to-noise (SNR) ratio ($> 3 : 1$) to measure phase precisely, but short enough so as not to exceed the coherence time of the interferometer. (Note that the phase error is $\approx 1/\mathrm{SNR}$ radians.) Should one choose either too short or too long a time period for fringe fitting the reference channel data, noise will be introduced in the referencing procedure and lead to degraded maps. In some cases, the time required to achieve an adequate SNR exceeds the coherence time of the interferometer and phase referencing is not possible!

The procedure described above yields a table of fringe-rates and phases as a function of time for all interferometer baselines. Almost all phase fluctuations in this table can be thought of as caused by something happening at each antenna (i.e., antenna based), with little or no additional contribution that is specifically baseline, or correlator, dependent. In this case, a *reference* antenna can be chosen (somewhat arbitrarily) and individual antenna-based tables of phase fluctuations determined. These antenna-based tables will have the property that differencing the phases from antennas $i$ and $j$ will yield the phases observed on the $(i, j)$–baseline. In practice, one can directly solve for station-based reference phases via *global fringe fitting* techniques.

The final step in the calibration process involves using these antenna-based tables of visibility phase as a function of time to predict, and remove, the phase fluctuations on all interferometer baselines. The phase from the calibration table for antenna $i$ is interpolated to the time, $t_{data}$, of a visibility record in the full data base, yielding $\theta_i(t_{data})$. When performing this interpolation it is important to resolve integral turn ambiguities between entries in the reference feature phase table (see figure 11.7). One can then phase reference all the data for the baseline from the $i^{th}$ to the $j^{th}$ antenna, $S_{ij}(t_k, \nu_n)$, as follows:

$$S_{ij}(t_k, \nu_n) \leftarrow S_{ij}(t_k, \nu_n)\ e^{-i(\theta_i - \theta_j)}, \tag{11.12}$$

At this point we have completed the calibration of the spectral-line data and mapping can proceed.

## 11.4 Fringe-Rate Mapping

Once the data are calibrated, one can often proceed to construct line-channel maps in a manner similar to that for continuum sources. However, what if one

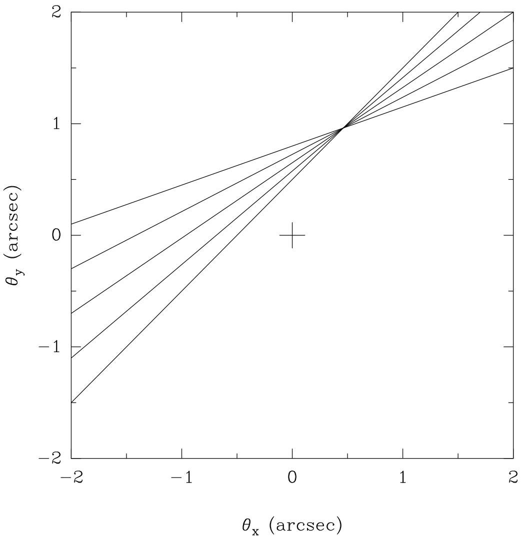


**Figure 11.8:** Fringe-rate mapping. Shown is a 4 arcsec square field of the sky. The origin of the field, indicated by the cross, is the location of the emission from the channel used to phase reference the data. Each line on the figure gives positions on the sky consistent with a fringe-rate measurement in a single spectral channel at a given time on one interferometer baseline. Measurements at different times or on multiple baselines result in lines of different orientation, and the intersections of the lines locates the position of the emission.

has very limited data? For example, data from a few baselines or data with poor amplitude calibration are difficult to analyze via standard synthesis mapping techniques. In addition, what if one has emission spread over a very large (and possibly unknown) field on the sky? For example, the $H_2O$ masers in the Orion-KL region are found over a 40 × 40 arcsec field. Using an interferometer with a synthesized beam of 1 mas, and mapping with 3 pixels per beam, would require maps with $120,000 \times 120,000$ pixels! Currently this is computationally "challenging".

For the reasons outlined above, one often wants a "first cut" or crude mapping technique that is not very sensitive to $(u, v)$ coverage or amplitude calibration. One such technique is called fringe-rate mapping. Fringe-rate mapping makes use of the fact that a single fringe-rate measurement (determined by fringe fitting data in a spectral channel at a given time and on a given baseline) constrains the location of the dominant emission to a "line" on the sky. Figure 11.8 gives an example of 5 such fringe-rate lines; these lines might come from 5 scans on one baseline or from 1 scan on 5 baselines. The intersection of the fringe-rate lines indicates the location of the emission (relative to the position of the emission used to phase reference the data).

With fringe-rate mapping, one can map large fields with a modest computational resources. Amplitude calibration is not necessary, since such calibration does not strongly affect fringe rate estimates for most fringe fitting algorithms. Typical accuracies of fringe-rate mapping for strong $H_2O$ masers are $\sim 1$ mas. Note, however, that as for synthesis mapping, limited time or baseline coverage often leads to limited positional accuracy. In the example shown in figure 11.8, positional accuracy is better perpendicular to the fringe-rate lines (from the upper-left to lower-right) and poorer along the fringe-rate lines.

## References

Thompson, A. R., Moran, J. M., & Swenson, G. W., Jr. 1986. *Interferometry and Synthesis in Radio Astronomy*. New York: Wiley-Interscience. First (1991) and second (1994) reprintings by Krieger Pub. Co., Malabar (Florida).